Turbulent statistics and intermittency enhancement in coflowing superfluid ^{4}He

L. Biferale,[1] D. Khomenko,[2,3] V. L'vov,[2] A. Pomyalov,[2] I. Procaccia,[2] and G. Sahoo[4]
[1]*Department of Physics and INFN, University of Rome, Tor Vergata, 00133 Roma, Italy*
[2]*Department of Chemical Physics, Weizmann Institute of Science, 7610001 Rehovot, Israel*
[3]*Laboratoire de physique théorique, Département de physique de l'ENS, École normale supérieure, PSL Research University, Sorbonne Universités, UPMC Université Paris 06, CNRS, 75005 Paris, France*
[4]*Department of Mathematics and Statistics and Department of Physics, University of Helsinki, FI-00014 Helsinki, Finland*

(Received 21 November 2017; published 21 February 2018)

The large-scale turbulent statistics of mechanically driven superfluid ^{4}He was shown experimentally to follow the classical counterpart. In this paper, we use direct numerical simulations to study the whole range of scales in a range of temperatures $T \in [1.3, 2.1]$ K. The numerics employ self-consistent and nonlinearly coupled normal and superfluid components. The main results are that (i) the velocity fluctuations of normal and super components are well correlated in the inertial range of scales, but decorrelate at small scales. (ii) The energy transfer by mutual friction between components is particulary efficient in the temperature range between 1.8 and 2 K, leading to enhancement of small-scale intermittency for these temperatures. (iii) At low T and close to T_λ, the scaling properties of the energy spectra and structure functions of the two components are approaching those of classical hydrodynamic turbulence.

DOI: 10.1103/PhysRevFluids.3.024605

I. INTRODUCTION

Superfluid ^{4}He below the transition temperature $T_\lambda = 2.17$ K may be viewed as a two-fluid system [1–3] consisting of a normal fluid with very low kinematic viscosity $\nu_n(T)$ and an inviscid superfluid component. The contributions of the components are defined by their densities, $\rho_n(T), \rho_s(T)$, constituting together the density of superfluid ^{4}He: $\rho_{He} = \rho_n(T) + \rho_s(T)$. Each component moves with its own velocity $u_n(\boldsymbol{r},t), u_s(\boldsymbol{r},t)$. Due to quantum mechanical restrictions, the circulation in the superfluid component is confined to thin vortex lines and quantized to multiples of circulation quantum $\kappa = h/m \approx 10^{-3}\,\mathrm{cm}^2/\mathrm{s}$, where h is the Plank constant and m denotes the mass of a ^{4}He atom. The turbulence in the superfluid component takes the form of a dense disordered tangle of these vortex lines with a typical intervortex distance ℓ.

It is commonly accepted that the statistical properties of the large-scale fluctuation in turbulent superfluid He conform with those of classical fluids when forced by mechanical means. Examples are rotating containers or flows behind a grid. The mean velocities of the normal and superfluid components in such driven superfluid ^{4}He appear to coincide [4]. Numerous laboratory and theoretical studies showed that under these conditions the mutual friction between the normal and superfluid components couples also their fluctuations: $u_n(\boldsymbol{r},t) \approx u_s(\boldsymbol{r},t)$ almost at all scales and the resulting turbulent energy spectra of the mechanically driven superfluid turbulence are close to those of the classical hydrodynamic turbulence [1,5–9]. Experiments utilizing solid hydrogen particles to visualize the inertial range of scales [10] found that the probability distribution functions of the particle velocities and velocity increments are similar to those of viscous flows.

One of the important aspects of the turbulent statistics in classical turbulence is the intermittency of the velocity fluctuations. This intermittency results in corrections to the dimensionally derived

energy spectra and structure functions. This subject is thoroughly studied in the classical case, but much less so in the context of superfluid ^{4}He. The experiments [5–7], conducted mostly at low temperatures and close to T_λ, did not find deviations from the turbulent statistics of classical flows. A very recent experimental study [11] of turbulence in the wake of a disk was conducted in a wide range of temperatures; it also did not find any temperature dependence of the scaling exponent of the second-order structure function. The experimental study [12] of turbulence behind a grid indicated a temperature dependence of higher order structure functions scaling. Stronger than classical intermittency was detected also in the preliminary studies in Large cryogenic Von Karman facility in Grenoble (SHREK) [13]. The particle velocity distributions and flatness at scales smaller than the intervortex distance showed [14,15] that measures of intermittency grow with decreasing scales for both thermally and mechanically driven superfluid ^{4}He. This effect was attributed to the interaction between particles and quantum vortices and therefore interpreted as a signature of the quantum nature of the flow.

Numerical simulations of homogeneous isotropic superfluid turbulence using different methods indicated that turbulence statistics in ^{4}He depend on the temperature. The important aspect is the relative density of the normal and super components. At temperature close to the T_λ and also for $T \lesssim 1.6$ K, where one or the other component dominate, the scaling exponents of structure functions are close to those of classical turbulence. In the range of temperatures where the densities of the components are similar, the statistics change. The shell-model study [16] found larger intermittency corrections compared to classical turbulence in these conditions. It was conjectured that the effect is related to the energy exchange between the normal and superfluid components and the additional dissipation due to mutual friction between components. Recently, these findings were questioned in another shell-model study [17], where intermittency was found to be suppressed for the same conditions or even absent in a certain temperature range. This conjecture appears to disagree with the results of the Gross-Pitaevkii simulations [18] of grid turbulence. There enhanced intermittency is found in the zero-temperature limit. In light of these conflicting results, it appears worthwhile to investigate these issues further.

We present here results of direct numerical simulations (DNS) of mechanically driven superfluid ^{4}He. We study energy spectra and structure functions of both components in a wide range of temperatures, using typical parameters [19] for ^{4}He. A nonmonotonic temperature dependence of the apparent scaling exponents of the energy spectra and the structure functions is found. The exponents are close to their classical counterparts at low temperatures and close to T_λ. In the intermediate temperature range $1.8 \lesssim T \lesssim 2$ K, where the densities of the components are similar $\rho_s \sim \rho_n$, the scaling properties significantly deviate from their classical values. The difference in properties can be attributed to the degree of dynamical correlations between the fluctuations of the two components. The normal and superfluid velocity fluctuations appear correlated at low and high temperatures, but almost uncorrelated in the intermediate temperature range. Then the small-scale intermittency measured by the velocity flatness is found to strongly exceed the classical values. The analysis of the energy balance at different scales revealed the role of the dissipation by mutual friction in intermittency enhancement.

II. STATISTICS OF TURBULENCE IN COFLOWING ^{4}He: ANALYTICAL DESCRIPTION

A. Gradually damped HVBK equations for superfluid ^{4}He turbulence

Following Ref. [20], we describe large-scale turbulence in superfluid ^{4}He by the gradually damped version [16] of the coarse-grained Hall-Vinen [2]–Bekarevich-Khalatnikov [3] (HVBK) equations. It has the form of two Navier-Stokes equations for $\boldsymbol{u}_n(\boldsymbol{r},t)$ and $\boldsymbol{u}_s(\boldsymbol{r},t)$:

$$\frac{\partial \boldsymbol{u}_s}{\partial t} + (\boldsymbol{u}_s \cdot \nabla)\boldsymbol{u}_s - \frac{1}{\rho_s}\nabla p_s = \nu_s \Delta \boldsymbol{u}_s + \boldsymbol{f}_{ns} + \boldsymbol{\varphi}_s, \tag{1a}$$

$$\frac{\partial \boldsymbol{u}_{\rm n}}{\partial t} + (\boldsymbol{u}_{\rm n}\cdot\nabla)\boldsymbol{u}_{\rm n} - \frac{1}{\rho_{\rm n}}\nabla p_{\rm n} = \nu_{\rm n}\,\Delta\boldsymbol{u}_{\rm n} - \frac{\rho_{\rm s}}{\rho_{\rm n}}\boldsymbol{f}_{\rm ns} + \boldsymbol{\varphi}_{\rm n}, \tag{1b}$$

$$p_{\rm n} = \frac{\rho_{\rm n}}{\rho}\Big[p + \frac{\rho_{\rm s}}{2}|\boldsymbol{u}_{\rm s}-\boldsymbol{u}_{\rm n}|^2\Big], \quad p_{\rm s} = \frac{\rho_{\rm s}}{\rho}\Big[p - \frac{\rho_{\rm n}}{2}|\boldsymbol{u}_{\rm s}-\boldsymbol{u}_{\rm n}|^2\Big],$$

$$\boldsymbol{f}_{\rm ns} \simeq \Omega\,(\boldsymbol{u}_{\rm n}-\boldsymbol{u}_{\rm s}), \quad \Omega = \alpha(T)\,\Omega_{\rm T}, \tag{1c}$$

stirred by a random force $\boldsymbol{\varphi}(\boldsymbol{r},t)$ and coupled by the mutual friction force $\boldsymbol{f}_{\rm ns}$ in approximated form [21], Eq. (1c). It involves the temperature-dependent dimensionless dissipative mutual friction parameter $\alpha(T)$ and the characteristic vorticity, denoted as $\Omega_{\rm T}$. From a microscopic point of view, $\Omega_{\rm T}$ is related to the quantized vortex line density $\mathcal{L}$: $\Omega_{\rm T} = \kappa\,\mathcal{L}$. Although there is no generally accepted equation that relates $\kappa\mathcal{L}$ and the vorticity field $\boldsymbol{\omega}(\boldsymbol{r},t) = \nabla\times\boldsymbol{u}_{\rm s}(\boldsymbol{r},t)$, there are a few different ways to estimate $\Omega_{\rm T}$ in terms of $\boldsymbol{\omega}(\boldsymbol{r},t)$. We adopt here an approach of Stalp *et al.* [22] and approximate $\kappa\mathcal{L}$ as $C\sqrt{\langle|\boldsymbol{\omega}(\boldsymbol{r},t)|^2\rangle}$ with a dimensionless parameter $C\sim 1$ that depends on the vortex line polarization [23]. For the problem studied here, the particular value of C is not important and we estimate $\Omega_{\rm T}$ as follows [21]:

$$\Omega_{\rm T}^2(t) \approx \tfrac{1}{2}\langle|\boldsymbol{\omega}(\boldsymbol{r},t)|^2\rangle_{\boldsymbol{r}}. \tag{2a}$$

In isotropic turbulence studied here,

$$\langle|\boldsymbol{\omega}(\boldsymbol{r},t)|^2\rangle_{\boldsymbol{r}} = 2\int k^2 E_{\rm s}(k,t)dk, \tag{2b}$$

giving a simple estimate

$$\Omega_{\rm T}^2(t) \approx \int k^2 E_{\rm s}(k,t)dk. \tag{2c}$$

Here $E_{\rm s}(k,t)$ is the one-dimensional (1D) energy spectrum, normalized such that the total energy density per unit mass $\mathcal{E}_{\rm s}(t) = \int E_{\rm s}(k,t)\,dk$. The turbulent vorticity $\Omega_{\rm T}(t)$ is then defined self-consistently from the instantaneous energy spectrum $E_{\rm s}(k,t)$.

Other parameters include the pressures $p_{\rm n}$, $p_{\rm s}$ of the normal and the superfluid components, the He density $\rho \equiv \rho_{\rm s}+\rho_{\rm n}$, and the kinematic viscosity of normal fluid component $\nu_{\rm n} = \eta/\rho_{\rm n}$, where η is dynamical viscosity of ^{4}He. The dissipative term with the Vinen's effective superfluid viscosity [24] $\nu_{\rm s}$ was added [16] to account for the energy dissipation at the intervortex scale ℓ due to vortex reconnections and similar effects. As shown in Refs. [25–27], this approximation is quite reasonable for $T \gtrsim 1$ K.

Generally speaking, Eqs. (1a) and (1b) involve also contributions of a reactive (dimensionless) mutual friction parameter α' that renormalizes their nonlinear terms, for example, in Eq. (1a) $(\boldsymbol{u}_{\rm s}\cdot\nabla)\boldsymbol{u}_{\rm s} \Rightarrow (1-\alpha')(\boldsymbol{u}_{\rm s}\cdot\nabla)\boldsymbol{u}_{\rm s}$. However, in the studied range of temperatures $|\alpha'| \lesssim 0.02 \ll 1$ [see column 6 in Table I] and this renormalization can be peacefully ignored. For similar reasons, we neglected all other α'-related term in Eqs. (1).

B. Statistical description of space-homogeneous, isotropic turbulence of superfluid ^{4}He

1. Definition of 1-D energy spectra and cross correlations

Traditionally, the energy distribution over scales in a space-homogeneous, isotropic case is described by one-dimensional (1D) energy spectra of the normal and superfluid components, $E_{\rm n}(k)$ and $E_{\rm s}(k)$:

$$E_{\rm n}(k) = \frac{k^2}{2\pi^2}F_{\rm nn}(k), \quad E_{\rm s}(k) = \frac{k^2}{2\pi^2}F_{\rm ss}(k), \tag{3a}$$

defined in terms of the three-dimensional spectra $F_{\rm nn}(k)$ and $F_{\rm ss}$:

$$\langle\widetilde{\boldsymbol{u}}_{\rm n}(\boldsymbol{k},t)\cdot\widetilde{\boldsymbol{u}}_{\rm n}(\boldsymbol{q},t)\rangle = (2\pi)^3 F_{\rm nn}(\boldsymbol{k})\,\delta(\boldsymbol{k}+\boldsymbol{q}), \tag{3b}$$

$$\langle\widetilde{\boldsymbol{u}}_{\rm s}(\boldsymbol{k},t)\cdot\widetilde{\boldsymbol{u}}_{\rm s}(\boldsymbol{q},t)\rangle = (2\pi)^3 F_{\rm ss}(\boldsymbol{k})\,\delta(\boldsymbol{k}+\boldsymbol{q}). \tag{3c}$$

TABLE I. Parameters of simulations by columns: (1) temperature (K); (2) ratio of the normal and superfluid densities, ρ_n/ρ_s; (3 and 4) the numerical kinematic viscosity of the superfluid and normal fluid components $\tilde{\nu}_s$ and $\tilde{\nu}_n$; (5 and 6) parameters of the mutual friction α and α'; (7 and 8) the root mean square (rms) of the superfluid and normal fluid turbulent velocity fluctuations u_T^s and u_T^n; (9 and 10) the rms of the superfluid and normal fluid vorticity Ω_T^s and Ω_T^n; (11) the intervortex distance $\ell = (\Omega_T^s/\bar{\kappa})^{-1/2}$; (12 and 13) the Taylor-microscale Reynolds number of the superfluid and normal fluid components Re_λ^s and Re_λ^n, where $\lambda_{n,s} = 2\pi\sqrt{\langle u_{n,s}{}^2\rangle/\langle\omega_{n,s}{}^2\rangle}$ is the Taylor microscale. For details see Sect. III A. In all simulations, the number of collocation points along each axis is $N = 1024$, the size of the periodic box is $L = 2\pi$, and the range of forced wave numbers $k^{\bar{\varphi}} = [0.5, 1.5]$.

1	2	3	4	5	6	7	8	9	10	11	12	13
T	$\frac{\rho_s}{\rho_n}$	$\tilde{\nu}_s$ $\times 10^4$	$\tilde{\nu}_n$ $\times 10^4$	α $\times 10$	α' $\times 10$	$u_T^n = \sqrt{\langle u_n{}^2\rangle}$	$u_T^s = \sqrt{\langle u_s{}^2\rangle}$	$\Omega_T^n = \sqrt{\langle\omega_n{}^2\rangle/2}$	$\Omega_T^s = \sqrt{\langle\omega_s{}^2\rangle/2}$	$\ell =$ $\times 10^3$	$\mathrm{Re}_\lambda^n = u_T^n\lambda_n/\nu_n$	$\mathrm{Re}_\lambda^s = u_T^s\lambda_s/\nu_s$
1.3	20.0	5.0	117.0	0.34	0.14	4.3	4.5	33	62	8.9	210	2900
1.6	5.0	5.0	13.5	0.97	0.16	4.2	4.2	45	57	6.5	1300	2700
1.8	2.17	5.0	6.1	1.6	0.08	3.6	3.6	31	37	7.6	3000	3100
1.9	1.35	6.3	5.0	2.06	0.08	3.7	3.7	30	30	8.7	4100	3200
1.9	1.35	5.0	4.0	2.06	0.08	3.4	3.5	31	31	7.6	4100	3500
2.0	0.81	8.6	5.0	2.79	0.12	3.5	3.5	24	21	11	4500	3000
2.0	0.81	5.0	3.0	2.79	0.12	3.3	3.3	21	18	9.4	7700	5400
2.1	0.35	12.5	5.0	4.81	−0.24	3.6	3.5	35	25	11	3300	1700
2.1	0.35	5.0	2.0	4.81	−0.24	4.3	4.2	70	52	4.7	5900	3000

Here $\widetilde{\boldsymbol{u}}_n(\boldsymbol{k},t)$ and $\widetilde{\boldsymbol{u}}_s(\boldsymbol{k},t)$ are $\boldsymbol{k}$-Fourier transforms of the velocity fields $\boldsymbol{u}_n(\boldsymbol{r},t)$ and $\boldsymbol{u}_s(\boldsymbol{r},t)$. Delta function $\delta(\boldsymbol{k}+\boldsymbol{q})$ is a consequence of space homogeneity.

Similarly to the energy spectra, we define a simultaneous cross-correlation function:

$$E_{ns}(k) \equiv \frac{k^2}{2\pi^2} F_{ns}(k), \tag{4a}$$

$$\langle \widetilde{\boldsymbol{u}}_n(\boldsymbol{k},t)\cdot\widetilde{\boldsymbol{u}}_s(\boldsymbol{q},t)\rangle = (2\pi)^3 F_{ns}(\boldsymbol{k})\,\delta(\boldsymbol{k}+\boldsymbol{q})\,, \tag{4b}$$

and a third-order correlation function

$$\left\langle \widetilde{u}_s^{\xi}(\boldsymbol{k},t)\,\widetilde{u}_s^{\beta}(\boldsymbol{q},t)\,\widetilde{u}_s^{\gamma}(\boldsymbol{p},t)\right\rangle = (2\pi)^3 F_{sss}^{\xi\beta\gamma}(\boldsymbol{k},\boldsymbol{q},\boldsymbol{p})\,\delta(\boldsymbol{k}+\boldsymbol{q}+\boldsymbol{p}). \tag{5}$$

2. Energy balance equation in the k representation

The balance equations [28] for superfluid and normal fluid energy spectra, $E_s(k,t)$ and $E_n(k,t)$, in the stationary case read

$$\frac{\partial\varepsilon_s(k)}{\partial k} + D_{s,\nu}(k) + D_{s,\alpha}(k) = 0, \tag{6a}$$

$$\frac{\partial\varepsilon_n(k)}{\partial k} + D_{n,\nu}(k) + D_{n,\alpha}(k) = 0, \tag{6b}$$

$$D_{s,\nu}(k) = 2\,\nu_s k^2 E_s(k), \quad D_{n,\nu} = 2\,\nu_n k^2 E_n(k), \tag{6c}$$

$$D_{s,\alpha}(k) = 2\,\Omega[E_s(k) - E_{ns}(k)], \tag{6d}$$

$$D_{n,\alpha}(k) = 2\,\Omega\frac{\rho_s}{\rho_n}[E_n(k) - E_{ns}(k)]. \tag{6e}$$

Here terms $D_{s,\nu}$ and $D_{n,\nu}$ describe viscous energy dissipation. The terms $D_{s,\alpha}$ and $D_{n,\alpha}$ are responsible for the energy dissipation by mutual friction with characteristic frequency Ω given by Eqs. (1c) and (2).

To obtain a simple form of Eqs. (6d) and (6e), we, following Ref. [21], accounted for the fact that $\Omega(t)$ is dominated by the motions of smallest scales (about intervortex distance ℓ), while $E(k,t)$ is dominated by the $1/k$ scale. This allows us to neglect their correlation in time and to replace $\langle\Omega(t)E(k,t)\rangle$ by a product of $\langle\Omega(t)\rangle_t = \Omega$ and $\langle E(k,t)\rangle_t = E(k)$.

First terms of the balance equations are related to the energy transfer over scales. The energy transfer term $\mathrm{Tr}(k)$ in Eqs. (6) (in which we omit here subscripts "$_{\mathrm{s}}$" and "$_{\mathrm{n}}$") originates from the nonlinear terms in the HVBK Eqs. (1a) and has the same form as in classical hydrodynamic turbulence (see, e.g., Refs. [29,30]):

$$\mathrm{Tr}(\boldsymbol{k}) = 2\,\mathrm{Re}\left\{\int V^{\xi\beta\gamma}(\boldsymbol{k},\boldsymbol{q},\boldsymbol{p})\,F^{\xi\beta\gamma}(\boldsymbol{k},\boldsymbol{q},\boldsymbol{p})\delta(\boldsymbol{k}+\boldsymbol{q}+\boldsymbol{p})\frac{d^3q\,d^3p}{(2\pi)^6}\right\}, \tag{7a}$$

$$V^{\xi\beta\gamma}(\boldsymbol{k},\boldsymbol{q},\boldsymbol{p}) = i\left(\delta_{\xi\xi'} - \frac{k^\xi k^{\xi'}}{k^2}\right)(k^\beta\delta_{\xi'\gamma} + k^\gamma\delta_{\xi'\beta}). \tag{7b}$$

Importantly, $\mathrm{Tr}(k)$ preserves total turbulent kinetic energy $\int_0^\infty \mathrm{Tr}(k')dk' = 0$ and therefore can be written in the 1D divergent form,

$$\mathrm{Tr}(k) = \frac{\partial\,\varepsilon(k)}{dk}, \tag{7c}$$

where $\varepsilon(k)$ is the energy flux over scales.

C. Generalized Kolmogorov's $\frac{4}{5}$ law for superfluid turbulence

One of the best-known results in the statistical theory of the homogeneous, stationary, isotropic, fully developed hydrodynamic turbulence is Kolmogorov's "four-fifth law" [31], which relates the third-order structure function

$$S_3^{\mathrm{l}}(R) = \langle[\delta u^{\mathrm{l}}(\boldsymbol{r},\boldsymbol{R})]^3\rangle \tag{8a}$$

of the longitudinal velocity differences

$$\delta u^{\mathrm{l}}(\boldsymbol{r},\boldsymbol{R}) \equiv \delta\boldsymbol{u}(\boldsymbol{r},\boldsymbol{R})\cdot\boldsymbol{R}/R, \tag{8b}$$

$$\delta\boldsymbol{u}(\boldsymbol{r},\boldsymbol{R}) \equiv [\boldsymbol{u}(\boldsymbol{r}+\boldsymbol{R}) - \boldsymbol{u}(\boldsymbol{r})], \tag{8c}$$

to the rate of energy dissipation ε. Note that we omitted for brevity the time argument t in notations for the velocity field $\boldsymbol{u}(\boldsymbol{r},t)$ and the correlation functions. In the inertial interval of scales, this law reads

$$S_{3,\mathrm{l}}(R) = -\tfrac{4}{5}\,\varepsilon R. \tag{9}$$

Formulated in the $\boldsymbol{R}$ space, Eq. (9) is much simpler than its equivalent Eqs. (7) in the $\boldsymbol{k}$ representation that relates the third-order correlation function $\boldsymbol{F}_{\mathrm{sss}}(\boldsymbol{k},\boldsymbol{q},\boldsymbol{p})$, Eq. (5), to the energy flux $\varepsilon(k)$.

To generalize the $\frac{4}{5}$ law (9) to the case of superfluid turbulence, define the second-order velocity structure functions of the normal and superfluid velocity differences [32]

$$S_{\mathrm{s}}(\boldsymbol{R}) = \langle|\delta\boldsymbol{u}_{\mathrm{s}}(\boldsymbol{r},\boldsymbol{R})|^2\rangle, \tag{10a}$$

$$S_{\mathrm{n}}(\boldsymbol{R}) = \langle|\delta\boldsymbol{u}_{\mathrm{n}}(\boldsymbol{r},\boldsymbol{R})|^2\rangle, \tag{10b}$$

and triple correlations

$$J_{\mathrm{s}}^{\alpha,\beta\gamma}(\boldsymbol{R}) = \left\langle u_{\mathrm{s}}^\alpha(\boldsymbol{R}+\boldsymbol{r})u_{\mathrm{s}}^\beta(\boldsymbol{r})u_{\mathrm{s}}^\gamma(\boldsymbol{r})\right\rangle, \tag{10c}$$

$$J_{\mathrm{n}}^{\alpha,\beta\gamma}(\boldsymbol{R}) = \left\langle u_{\mathrm{n}}^\alpha(\boldsymbol{R}+\boldsymbol{r})u_{\mathrm{n}}^\beta(\boldsymbol{r})u_{\mathrm{n}}^\gamma(\boldsymbol{r})\right\rangle. \tag{10d}$$

From now on, we omit subscripts "$_{\rm n}$" or "$_{\rm s}$" in relations that are valid for both normal and superfluid components. We also assume spatial homogeneity and $\boldsymbol{R} \Leftrightarrow -\boldsymbol{R}$ symmetry (i.e., absence of helicity). In that case, Eqs. (10a) and (10b) can be rewritten as follows:

$$S(\boldsymbol{R}) = -2\,\langle \delta\boldsymbol{u}(\boldsymbol{r},\boldsymbol{R}) \cdot \boldsymbol{u}(\boldsymbol{r})\rangle. \tag{10e}$$

Similarly, the equations for the third-order structure function $\langle \delta u^{\alpha}(\boldsymbol{r},\boldsymbol{R})\delta u^{\beta}(\boldsymbol{r},\boldsymbol{R})\delta u^{\gamma}\,(\boldsymbol{r},\boldsymbol{R})\rangle$ can be expressed via triple correlations (10c) and (10d). In the stationary turbulence, the velocity structure function (10e) is time independent. Computing its rate of change using Eqs. (1), we find

$$0 = \frac{\partial S(\boldsymbol{R})}{2\,\partial t} = -T(\boldsymbol{R}) + P(\boldsymbol{R}) - D_{\nu}(\boldsymbol{R}) - D_{\alpha}(\boldsymbol{R}). \tag{11a}$$

Here the energy transfer term $T(\boldsymbol{R})$ originates from the nonlinear term $(\boldsymbol{u}\cdot\boldsymbol{\nabla})\boldsymbol{u}$ in Eqs. (1), the energy pumping term $P(\boldsymbol{R})$ is from the random driving force $\boldsymbol{\varphi}(\boldsymbol{r},t)$, and the dissipation terms $D_{\nu}(\boldsymbol{R})$ and $D_{\alpha}(\boldsymbol{R})$ are from the viscous ($\propto\nu$) and the mutual friction ($\propto\alpha$) terms.

Taking into account that due to space homogeneity, the one-point contribution vanishes [32], the transfer term may be written as

$$\begin{aligned} T(\boldsymbol{R}) &= 2\left\langle u^{\alpha}(\boldsymbol{r}+\boldsymbol{R})\frac{\partial}{\partial r^{\beta}}\,u^{\beta}(\boldsymbol{r})u^{\alpha}(\boldsymbol{r})\right\rangle = -2\left\langle u^{\beta}(\boldsymbol{r})u^{\alpha}(\boldsymbol{r})\frac{\partial}{\partial r^{\beta}}u^{\alpha}(\boldsymbol{r}+\boldsymbol{R})\right\rangle \\ &= -2\left\langle u^{\beta}(\boldsymbol{r})u^{\alpha}(\boldsymbol{r})\frac{\partial}{\partial R^{\beta}}u^{\alpha}(\boldsymbol{r}+\boldsymbol{R})\right\rangle = -2\,\frac{\partial J^{\alpha,\beta\alpha}(\boldsymbol{R})}{\partial R^{\beta}}. \end{aligned} \tag{11b}$$

Here summation over repeated indices is implied.

The rest of contributions to (11a) can be found straightforwardly:

$$P(\boldsymbol{R}) = 2\varepsilon\,, \quad D_{\nu}(\boldsymbol{R}) = \nu\nabla^2 S(\boldsymbol{R}), \tag{11c}$$

$$D_{\alpha,{\rm s}}(\boldsymbol{R}) = \Omega[S_{\rm ns}(\boldsymbol{R}) - S_{\rm s}(\boldsymbol{R})], \tag{11d}$$

$$D_{\alpha,{\rm n}}(\boldsymbol{R}) = \frac{\rho_{\rm s}}{\rho_{\rm n}}\,\Omega[S_{\rm ns}(\boldsymbol{R}) - S_{\rm n}(\boldsymbol{R})], \tag{11e}$$

$$S_{\rm ns}(\boldsymbol{R}) \equiv \langle \delta\boldsymbol{u}_{\rm s}(\boldsymbol{r},\boldsymbol{R}) \cdot \delta\boldsymbol{u}_{\rm n}(\boldsymbol{r},\boldsymbol{R})\rangle. \tag{11f}$$

Equations (11) can be rewritten in a compact form:

$$T(\boldsymbol{R}) = -2\,\boldsymbol{\nabla}\cdot\boldsymbol{J}(\boldsymbol{R}) = 2\varepsilon - \nu\nabla^2 S(\boldsymbol{R}) - D_{\alpha}(\boldsymbol{R}), \tag{12a}$$

$$\boldsymbol{J}(\boldsymbol{R}) \equiv \langle \boldsymbol{u}(\boldsymbol{r})[\boldsymbol{u}(\boldsymbol{r})\cdot\boldsymbol{u}(\boldsymbol{r}+\boldsymbol{R})]\rangle, \tag{12b}$$

where $D_{\alpha}(\boldsymbol{R})$ is given by Eq. (11d) or (11e). Equations (12) represent the generalized form of the Kolmogorov's $\frac{4}{5}$ law for superfluid turbulence.

To test its consistency with the original form, we consider (12) in the inertial interval of scales of the isotropic turbulence without helicity. First, we recall the most general form of $J^{\alpha,\beta\gamma}$ in that case [32]:

$$\begin{aligned} J^{\alpha,\beta\gamma} &= a_1(R)[\delta_{\alpha\beta}R^{\gamma} + \delta_{\alpha\gamma}R^{\beta} + \delta_{\beta\gamma}R^{\alpha}] + a_2(R)[\delta_{\alpha\beta}R^{\gamma} + \delta_{\alpha\gamma}R^{\beta} - 2\delta_{\beta\gamma}R^{\alpha}] \\ &\quad + a_3(R)[\delta_{\alpha\beta}R^{\gamma} + \delta_{\alpha\gamma}R^{\beta} + \delta_{\beta\gamma}R^{\alpha} - 5R^{\alpha}R^{\beta}R^{\gamma}/R^2]. \end{aligned} \tag{13a}$$

Incompressibility conditions result in two relations between three functions $a_1(R)$, $a_2(R)$, and $a_3(R)$:

$$\left(\frac{d}{dR} + \frac{5}{R}\right)a_3(R) = \frac{2}{3}\,\frac{d}{dR}[a_1(R) + a_2(R)], \tag{13b}$$

$$\left(\frac{d}{dR} + \frac{3}{R}\right)[5a_1(R) - 4a_2(R)] = 0. \tag{13c}$$

Using Eqs. (13) one can simplify Eq. (11b) for the transfer term:

$$T(R) = 2\,\frac{\partial}{\partial R^{\alpha}}\,R^{\alpha}[5a_1(R) + 2a_2(R)]. \tag{14}$$

In the inertial interval of scales [i.e., $D_{\alpha} = 0$ and $D_{v} = 0$], the term $T(R)$ is independent of R. This is possible if a_1 and a_2 are independent of R as well. Then from Eqs. (13b), (13c), and (14) together with $T(R) = 2\,\varepsilon$, we find

$$a_1 = -2\varepsilon/45, \quad a_2 = -\varepsilon/18, \quad a_3 = 0. \tag{15}$$

Together with Eq. (13a), this finally gives

$$J^{\alpha,\beta\gamma} = -\frac{\varepsilon}{10}\left(R^{\gamma}\delta_{\alpha\beta} + R^{\beta}\delta_{\alpha\gamma} - \frac{2}{3}R^{\alpha}\delta_{\beta\gamma}\right). \tag{16}$$

The longitudinal third-order structure function S_3^{l}, Eqs. (8), can be rewritten as follows:

$$S_3^{\mathrm{l}}(R) = 6\langle u^{\mathrm{l}}(\boldsymbol{r}+\boldsymbol{R})(u^{\mathrm{l}}(\boldsymbol{r}))^2\rangle = 6J^{z,zz}(R), \tag{17}$$

where $u^{\mathrm{l}}(\boldsymbol{r}+\boldsymbol{R}) = u(\boldsymbol{r}+\boldsymbol{R})\cdot\hat{z}\,, \hat{z} = \boldsymbol{R}/R$. Together with Eqs. (16), this gives the celebrated $\frac{4}{5}$ Kolmogorov's law (9).

III. STATISTICS OF ^{4}He TURBULENCE: DNS RESULTS AND THEIR ANALYSIS

A. Numerical procedure

We carried out a series of DNSs of coupled HVBK Eqs. (1) for normal and superfluid velocities for different temperatures T using a fully dealiased pseudospectral code with resolution 1024^3 collocation points in a triply periodic domain of size $L = 2\pi$. Table I summarizes the parameters used in simulations. The temperature dependencies of some parameters used in Eq. (1) [ratio of superfluid and normal fluid densities $\rho_{\mathrm{s}}/\rho_{\mathrm{n}}$, mutual friction parameters α and $\alpha\rho_{\mathrm{s}}/\rho_{\mathrm{n}}$, and the kinematic viscosities ν_{s} and ν_{n}] are shown in Fig. 1. The temperature dependence of $\rho_{\mathrm{s}}/\rho_{\mathrm{n}}$, ν_{n},α, and α' is taken according to Ref. [19] and ν_{s} according to Ref. [25].

To obtain steady-state evolution, velocity fields of the normal and superfluid components are stirred by two independent random Gaussian forcings:

$$\langle\tilde{\varphi}_u(\boldsymbol{k},t)\cdot\tilde{\varphi}_u^{*}(\boldsymbol{q},t')\rangle = \Phi(k)\delta(\boldsymbol{k}-\boldsymbol{q})\delta(t-t')\widehat{P}(\boldsymbol{k}), \tag{18}$$

where $\widehat{P}(\boldsymbol{k})$ is a projector assuring incompressibility and $\Phi(k) = \Phi_0 k^{-3}$; * stands for complex conjugation and the forcing amplitude Φ_0 is nonzero only in a given band of Fourier modes: $k^{\bar{\varphi}} \in [0.5,1.5]$. Time integration is performed using second-order Adams-Bashforth scheme with viscous term exactly integrated.

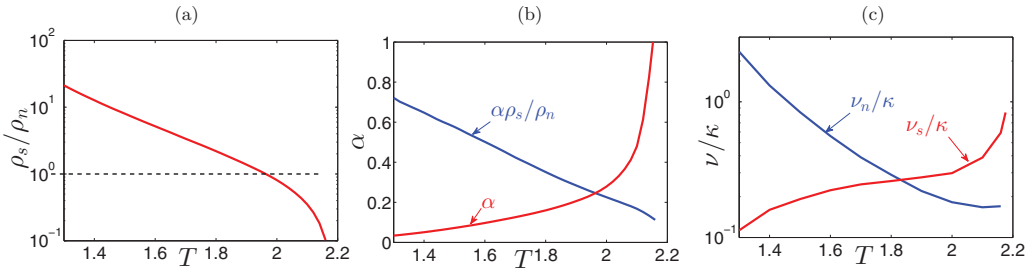

FIG. 1. Temperature dependence of ^{4}He parameters used in the simulations of HVBK Eqs. (1): ratio of the superfluid and normal fluid densities (a), mutual friction parameters α in the superfluid Eq. (1a) and $\alpha\rho_{\mathrm{s}}/\rho_{\mathrm{n}}$ in the normal fluid Eq. (1b) (b), and kinematic viscosities ν_{s} and ν_{n} (c).

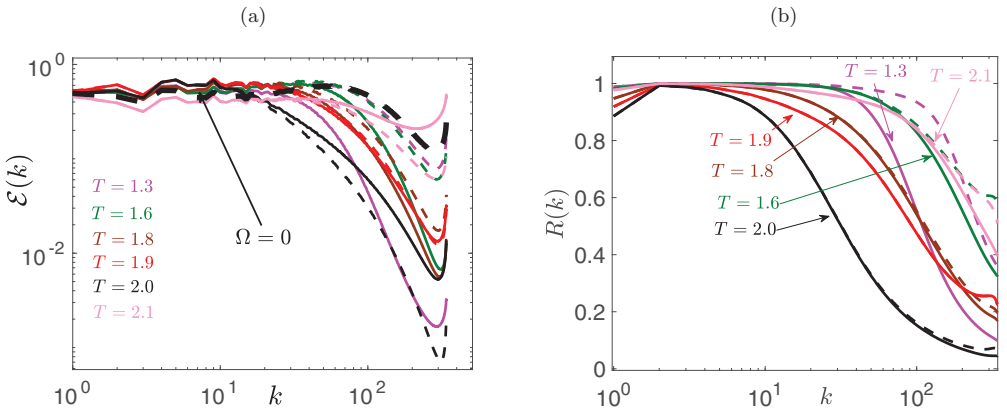

FIG. 2. (a) Normalized compensated by $k^{5/3}$ energy spectra of normal (solid line) and superfluid (dashed line) components $\mathcal{E}_{n,s}$ [Eq. (19)]. The thick black dashed line, marked $\Omega = 0$, corresponds to the energy spectra in the decoupled case. (b) Normalized cross-correlation functions $R_1(k)$ (solid lines) and $R_2(k)$ (dashed lines) [Eq. (21)].

Simulations for the temperature range $T = 1.3$–$2.1\,\mathrm{K}$ were carried out with the superfluid viscosity fixed $\tilde{\nu}_s = 5 \times 10^{-4}$ and the value of $\tilde{\nu}_n$ found using the known value of ratio ν_s/ν_n at each temperature. In addition, the simulations at low resolution (256^3) for $T = 1.7$–$2.1\,\mathrm{K}$ and at high resolution for high-temperature range $T = 1.8$–$2.1\,\mathrm{K}$ were carried out also with the constant viscosity of the normal fluid component and $\tilde{\nu}_s$ varied in accordance with the temperature dependence of their ratio. These additional simulations allowed us to distinguish the influence of the temperature dependence and the Reynolds number dependence of the structure functions and flatness of two components. When $\tilde{\nu}_s$ is constant and $\tilde{\nu}_n$ is varied, the results for normal component are affected by both dependencies, while the results for the superfluid component depend only on the temperature. Situation is reversed when $\tilde{\nu}_n$ is fixed and $\tilde{\nu}_s$ is varied: In this case, the results for the superfluid component depend simultaneously on the changing temperature and Reynolds number. Our exploratory results show that the outcome does not depend on the protocol. The detailed behavior needs to be explored further. We comment on this double dependence where relevant. The intervortex distance $\ell = (\Omega_r^s/\tilde{\kappa})^{-1/2}$ is estimated using the superfluid turbulent vorticity and the rescaled circulation quantum $\tilde{\kappa} = \kappa\tilde{\nu}_s/\nu_s$. In our simulations, the values of ℓ are at the edge of the real space resolution, while the wave numbers corresponding to the intervortex distance exceed our resolution at all temperatures.

B. Turbulent energy spectra

One-dimensional energy spectra for the normal fluid component (solid lines) and for the superfluid component (dashed lines) are shown in Fig. 2(a). The spectra are compensated by the Kolmogorov 1941 (K41) scaling behavior and normalized by the total kinetic energy of the normal fluid component:

$$\mathcal{E}_{n,s}(k) = k^{5/3} E_{n,s}(k)/E_n, \quad E_n = \int E_n(k)dk. \tag{19}$$

The line colors used for different temperatures from $T = 1.3\,\mathrm{K}$ to $T = 2.1\,\mathrm{K}$ are the same in all figures. For comparison, we also show in Fig. 1(a) by thick black dashed line the spectrum corresponding to the classical hydrodynamic turbulence. It was obtained by simulations of the decoupled Eqs. (1) with $\Omega = 0$ and equal viscosities.

There are several important features of these spectra. First of all, all the compensated spectra (both for normal and superfluid components) have a plateau in the small-k range, $k \lesssim 20$ for our resolution,

meaning that $E_s(k) \approx E_n(k) \propto k^{-5/3}$. We therefore confirm previous observations [1,4,5,7,8] that the energy spectra in the coflow of superfluid He are similar to the energy spectra observed in classical turbulence [33]. We do not resolve the intermittency corrections in the spectra.

For $k \gtrsim 20$, the compensated spectra for different temperatures fall off differently, due to combined influence of the viscous dissipation and dissipation by mutual friction. The interplay of these two types of dissipation leads to a complicated relation between the normal and superfluid spectra. Since $\nu_s < \nu_n$ for $T \lesssim 1.85\,\mathrm{K}$ and $\nu_s > \nu_n$ for $T \gtrsim 1.85\,\mathrm{K}$ [see Fig. 1(c) and Table I], the normal spectra (solid lines) decay faster than the superfluid spectra (dashed lines of the same color) for low temperatures and slower for high T, almost coinciding for $T = 1.9\,\mathrm{K}$ (red lines). In addition, all normal fluid spectra [solid lines in Fig. 2(a)] lie below the classical spectrum (thick black dashed line for $\Omega = 0$) for the same ν_n. The additional energy dissipation is caused by the mutual friction, which becomes important where the velocities of the components become unlocked. On a semiquantitative level, this behavior is similar to that found earlier in Ref. [25] using Sabra-shell model approximation.

C. Cross correlation of the normal and superfluid velocities

To better understand the behavior of the energy spectra at different temperatures, we consider correlation between normal and superfluid velocities. It is often assumed [24] that the normal and superfluid velocities are "locked" in the sense that

$$\boldsymbol{u}_n(\boldsymbol{r},t) = \boldsymbol{u}_s(\boldsymbol{r},t). \tag{20}$$

To quantify the statistical grounds for this assumption, we use the 1D cross-velocity correlation function $\mathcal{E}_{ns} \propto \langle \boldsymbol{u}_n(\boldsymbol{k}) \cdot \boldsymbol{u}_s(\boldsymbol{k}) \rangle$, Eqs. (4), normalized in two ways [25,28,34]:

$$R_1(k) = \frac{2\,\mathrm{Re}\{E_{ns}(k)\}}{E_s(k) + E_n(k)}, \tag{21a}$$

$$R_2(k) = \frac{\mathrm{Re}\{E_{ns}(k)\}}{\sqrt{E_s(k) \cdot E_n(k)}}. \tag{21b}$$

Here $\mathrm{Re}\{...\}$ denotes real part of a complex variable.

Both cross correlations are equal to unity for fully locked superfluid and normal velocities [in the sence of Eq. (20)], and both vanish if the velocities are statistically independent. However, if the velocities are proportional to each other

$$\widetilde{\boldsymbol{u}}_n(\boldsymbol{k},t) = C(k)\widetilde{\boldsymbol{u}}_s(\boldsymbol{k},t), \tag{22a}$$

with $C(k) \neq 1$, then $R_1(k) = 2C(k)/[C^2(k)+1] < 1$, while $R_2(k)$ is still equals to unity, $R_2(k) = 1$. In any case, $R_1(k) \leqslant R_2(k)$.

The cross correlations $R_1(k)$ and $R_2(k)$ are shown in Fig. 2(b) by solid and dashed lines, respectively, with the same color code for different T as in Fig. 2(a). Clearly, both $R_1(k)$ and $R_2(k)$ monotonically decrease with k and for some cases become significantly smaller than unity already at $k \approx 10$. For example, for $T = 2.0\,\mathrm{K}$ and $k > 50$, $R_1(k) \approx R_2(k) < 0.3$. Thus, the normal and superfluid velocities begin to decorrelate in the crossover region between inertial and viscous interval and are practically uncorrelated in the viscous subrange. For temperatures around $1.8 \div 2.0\,\mathrm{K}$, the normal and superfluid viscosities are similar and $R_1(k) \approx R_2(k)$ at all k.

On the other hand, for low and high T, $R_2(k)$ significantly exceeds $R_1(k)$, especially in the large-wave-number limit. This is best visible for $T = 1.3\,\mathrm{K}$. At this temperature, $\nu_n \simeq 25\nu_s$ and the normal fluid component is overdamped at large k: $v_n(k) \ll v_s(k)$. As a result, $v_n(k)$ does not have its own nonlinear dynamics. Accounting in Eq. (1b) (in $\boldsymbol{k}$ representation) only for the viscous and mutual friction terms we find that

$$\nu_n k^2 \widetilde{\boldsymbol{u}}_n(\boldsymbol{k},t) \approx \frac{\alpha\rho_s\Omega}{\rho_n}\widetilde{\boldsymbol{u}}_s(\boldsymbol{k},t)\,, \tag{22b}$$

meaning that the normal fluid velocity follows the superfluid one in the sense of Eq. (22a) with

$$C(k) = \frac{\alpha \rho_s \Omega}{\rho_n \nu_n k^2} < 1. \tag{22c}$$

In this approximation, $E_n(k) \approx [C(k)]^2 E_s(k) < E_s(k)$ and $R_1(k) < 1$, while $R_2(k) \approx 1$. Similar (but less pronounced) effect takes place at temperatures near the T_λ, where $\nu_s \gg \nu_n$; see, for example, $R_1(k)$ and $R_2(k)$ in Fig. 2(b) for $T = 2.1$ K, for which $\nu_s \simeq 4\nu_s$. The fast change in the component's viscosity and density for $T > 2$ K [see Figs. 1(b) and 1(c)] leads to a striking difference in all statistical properties of superfluid ^{4}He at $T = 2$ K and $T = 2.1$ K, shown in the figures by black and pink lines, respectively.

We stress that numerical results shown in Fig. 2(b) qualitatively agree for most of temperatures with the analytical expression of the cross-correlation $E_{ns}(k)$ [25,34], which in current notations reads

$$\mathcal{E}_{ns}(k) = \frac{\alpha\, \Omega[\rho_n\, E_n(k) + \rho_s\, E_s(k)]}{\alpha\, \Omega\rho + \rho_n[(\nu_s + \nu_n)\, k^2 + \gamma_n(k) + \gamma_s(k)]}. \tag{23}$$

Here $\gamma_s(k) = \sqrt{k^3 E_s(k)}$ and $\gamma_n(k) = \sqrt{k^3 E_n(k)}$ are dimensional K-41 estimates of the turnover frequencies of eddies in the superfluid and normal fluid components, respectively.

D. Energy balance

To quantify the relative importance of different terms of the energy balance equations Eq. (6), we plot them in Fig. 3 for three typical temperatures $T = 1.3, 1.8$, and 2.1K together with the energy spectra E_s, E_n and the cross correlation E_{ns}. Here the terms $\langle \Omega(t) E(k,t) \rangle$ in Eqs. (6) were calculated directly, not using a product of averages.

Starting with low temperature [$T = 1.3$ K, Figs. 3(a) and 3(d)], we note that the normal and superfluid energy spectra and the cross correlation almost coincide for $k \lesssim 20$. For larger wave numbers, $E_n < E_{ns}$ and $D_{\alpha,n}$ is negative, transferring energy from the superfluid component to the normal component. Most of this energy is dissipated by the viscous friction $D_{\nu,n}$ even at low k. The

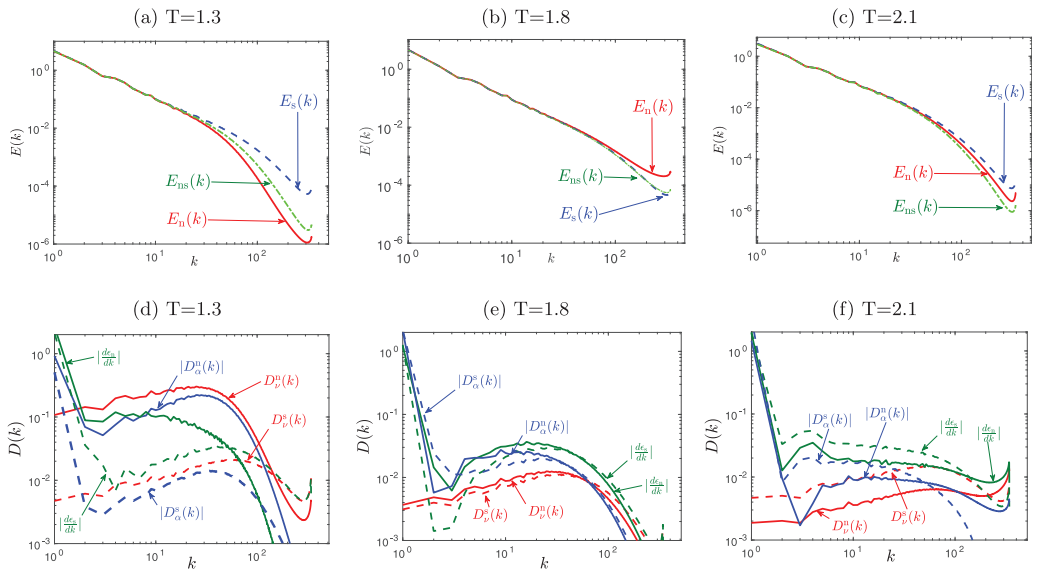

FIG. 3. Energy spectra [panels (a)–(c)] and the energy balance [panels (d)–(f)] for the normal (solid lines) and superfluid (dashed lines) components. The spectra and balances are shown for three representative temperatures. Different terms of Eq. (6) are marked in the panels. In panels (d)–(f), absolute values of the terms are shown.

normal component is mostly responsible for the energy dissipation at low T due to large ratio of densities and viscosity.

At moderate temperatures [$T = 1.8$ K, Figs. 3(b) and 3(e)], the two components have similar behavior. The energy exchange and dissipation due to mutual friction in both components is dominant over almost all scales, while viscous dissipation takes over only deep in the viscous k range.

At high T [Figs. 3(c) and 3(f)], the superfluid components is the most dissipative part of the system, by the mutual friction in the inertial range and by viscosity at higher k.

E. Velocity structure functions

Statistical properties of the turbulent flows are usually characterized by velocity structure functions $S_n(\boldsymbol{r})$. Their scaling behavior in the classical turbulence is well known. Much less is known about structure functions in the superfluid He. In this section, we discuss the velocity structure functions of normal and superfluid components as well as the flatness to analyze intermittency effects in the two-fluid system.

1. Third-order velocity structure functions S_3

One of the most solid results in hydrodynamics turbulence is the scaling of the third-order velocity structure function $S_3(\boldsymbol{r}) \propto \boldsymbol{r}$, which is a consequence of the $\frac{4}{5}$th law. To see in which sense this result is valid in the superfluid He, we plot in Fig. 4 the normalized $S_3(r)/r$ vs r for both components. First of all, we notice that the range of wave numbers, in which the expected scaling ($\propto r$) for classical (decoupled) case is observed, corresponds well to the scaling interval of the energy spectrum for this case. Very similar behavior is observed in S_3 of both components for the highest available temperature $T = 2.1$ K. At two lowest temperatures, $T = 1.3$ and 1.6 K, the superfluid structure function $S_{3,\mathrm{s}}$ almost coincides with the results for $T = 2.1$ K, while for the normal component $S_{3,\mathrm{n}}$ is closer to the moderate-temperature ones. This is the consequence of the combined influence of the temperature and Re-number dependence of the flow: The results presented here were obtained with fixed ν_s and for the superfluid component are affected only by temperature. The results for normal fluid obtained with fixed ν_n are very similar to shown here for the superfluid components, with the difference that the structure function for $T = 2.1$ K does not approach S_3 for the decoupled case.

For the moderate temperatures $T = 1.8$–2.0 K, the extent of the inertial interval where S_3/r is horizontal is shortened. For $T = 2.0$ K, there is no inertial scaling range at all, unlike the energy

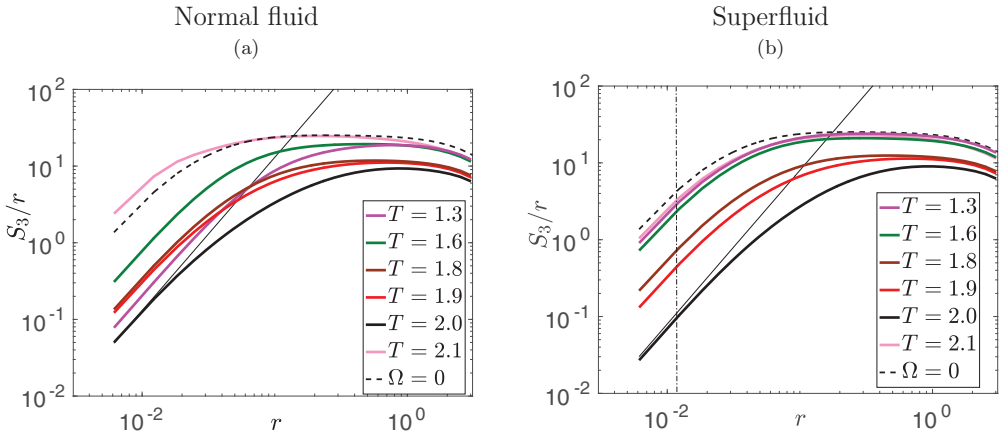

FIG. 4. The compensated structure functions $S_3(r)/r$ of normal (a) and superfluid (b) components as a function of r. Here and in other figures, the thick black dashed line, marked $\Omega = 0$, corresponds to the decoupled case. The thin straight solid lines indicate viscous behavior $S_3 \propto r^3$. The vertical thin dot-dashed straight lines in panel (b) marks the largest intervortex distance ℓ.

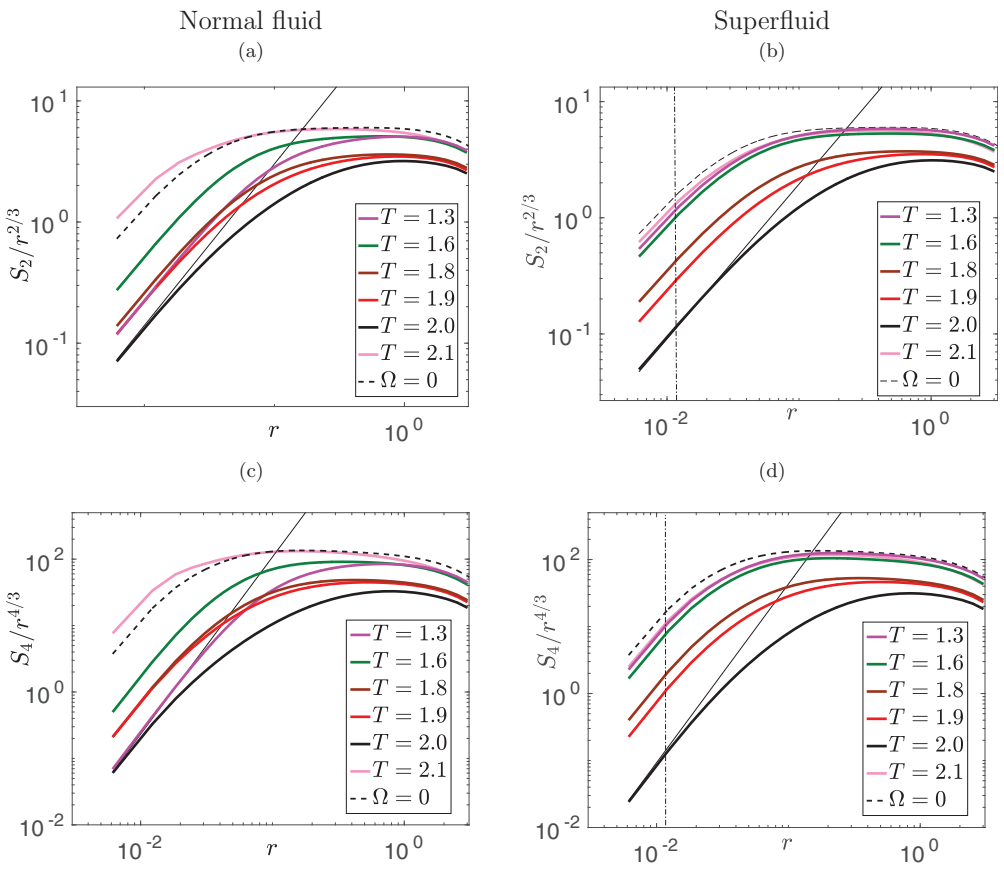

FIG. 5. The compensated structure functions $S_2(r)/r^{2/3}$ [panels (a) and (b)] and $S_4(r)/r^{4/3}$ [panels (c) and (d)] as a function of r. The thin straight solid lines indicate viscous behavior $S_2 \propto r^2$ and $S_4 \propto r^4$. The vertical thin dot-dashed straight lines in panels (b) and (d) mark the largest intervortex distance ℓ.

spectrum, in which the inertial range is clearly observed for $k \lesssim 20$. On the other hand, a viscous scaling range with scaling $\propto r^3$ at small r is observed in this temperature interval.

2. Velocity structure functions S_2 and S_4

Next we turn to the second- and fourth-order structure functions for both components. In Fig. 5 we plot S_2 and S_4 compensated by their respective Kolmogorov scaling. Clearly, all main features are similar to those of S_3; for low T and $T = 2.1$ K the structure functions of the superfluid component are similar to the classical case, while in the intermediate temperature range the inertial range scaling is lost with a scaling range for small r seen for $T = 2.0$ K. Here this scaling is $S_2(r) \propto r^2$ and $S_4(r) \propto r^4$ for both components and corresponds to the viscous range scaling. The signature of the mixed temperature and Re-number dependence in the normal fluid component is also very similar to that of the third-order structure function. We therefore can hope that using extended self-similarity [35] (ESS), i.e., using S_3 instead of r, will extend the scaling range and allow us to have better understanding of the intermittency corrections in superfluid turbulence.

3. Flatness and intermittency

The most direct information on the intermittency may be obtained from flatness $F_v \equiv S_4/S_2^2$. In Fig. 6, we show F_v for the normal and superfluid components as a function of S_3. Evidently, the

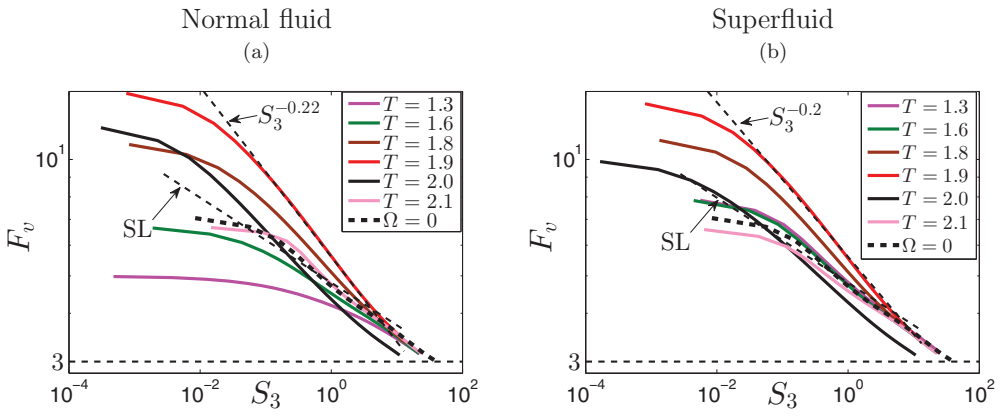

FIG. 6. Flatness of normal (a) and superfluid (b) components as a function of S_3. The horizontal dashed line correspond to $F_v = 3$. Note log-log scale. Thin straight dashed lines indicate the scaling, corresponding to the She-Leveque model of classical turbulence [36] (marked as "SL") and the fit for structure function at $T = 1.9$ K.

behavior of the flatness for the decoupled case resembles that of the classical turbulence: $F_v \approx 3$ at large scales and is larger for small scales, reaching the value of about 7 for $r \approx 10^{-2}$. Again, the flatness for both superfluid and normal components at low T and for $T = 2.1$K is close to the decoupled case, while in the intermediate-temperature regime the flatness grows faster toward small scales (with an apparent exponent -0.2 for $T = 1.9$ K compared to -0.14 for the decoupled case) and reaches values above 10. These observations confirm that intermittency in the intermediate range of temperatures is stronger that in classical turbulence.

Since accurate extraction of scaling exponents is difficult at our resolution, we plot in Fig. 7 the values of flatness at a number of normalized scales $\tilde{r}_{n,s} = r/\eta_{n,s}$, where $\eta_{n,s} = \sqrt{2}\tilde{\nu}_{n,s}/u_{rms}$, for different temperatures. The error bars were calculated by averaging the values of flatness obtained over different parts of the time realization. The horizontal dashed lines mark the values of flatness in the classical turbulence (represented here by the decoupled case). The color code of the lines indicated

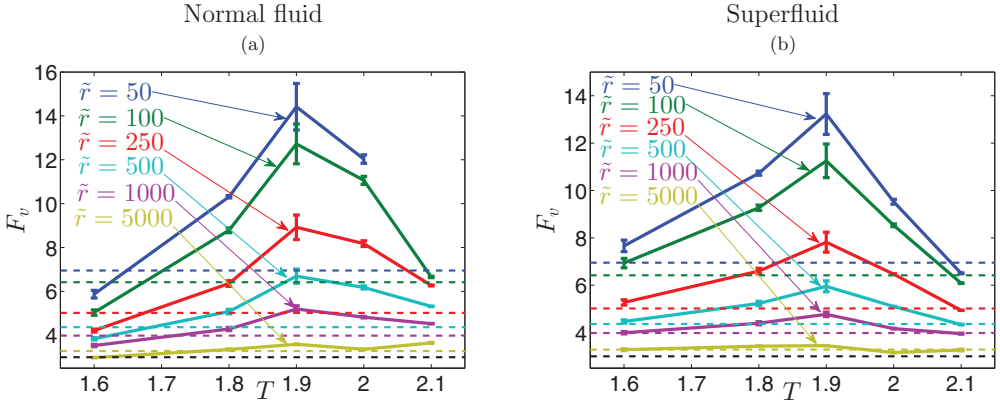

FIG. 7. Flatness as a function of temperature for the normal component (a) and for the superfluid component (b) for different separations $\tilde{r}_{n,s} = r/\eta_{n,s}$. The horizontal dashed lines lines correspond to the classical values of flatness for the same separations (marked by the same colors). The classical values are represented by the decoupled case. The lowest black dashed line corresponds to the Gaussian value $F_v = 3$. The error bars were obtained by averaging results for different intervals of the time realization.

the scale for which F_v was calculated. Clearly, the deviation from Gaussianity is close to that in the classical hydrodynamic turbulence at large scales and stronger for small scales. This intermittency enhancement is particulary notable for $T = 1.8$–$2.0\,\mathrm{K}$, with small-scale flatness exceeding twice the classical values for both components. The smaller than classical values of F_v for normal component at $T = 1.6\,\mathrm{K}$ are due to mixed influence of temperature and Re number dependence of the structure functions. These values are similar to F_v for superfluid component when calculated with fixed $\tilde{\nu}_n$, although the error bars in this case are larger.

F. Flip-flop scenario of the intermittency enhancement in ^{4}He turbulence

The intermittency enhancement, clearly demonstrated in Fig. 7, takes place at temperatures for which properties of normal and superfluid components are very similar. Closeness of densities leads to most efficient energy exchange by mutual friction. Indeed, the dissipation by mutual friction is almost identical at $T = 1.8\,\mathrm{K}$ (cf. Fig. 3) and is responsible for the energy dissipation in both components at almost all scales. We therefore suggest a variant of a *flip-flop scenario* [20] of the intermittency enhancement in ^{4}He turbulence by a random energy transfer between normal and superfluid components due to mutual friction. Such an energy exchange serves as additional random forcing in a wide range of scales, leading to enhanced intermittency of the velocity fluctuations.

IV. SUMMARY

We performed a series of DNS of the two-fluid gradually damped HVBK equations for homogeneous isotropic coflows in superfluid ^{4}He. The two fluid components are interacting via a self-consistent and nonlinear mutual friction, defined in terms of a temperature-dependent coupling factor which is a function of the superfluid enstrophy spectrum. The statistical properties of both components, characterized by energy spectra, velocity structure functions, and flatness, are similar, although not identical. We found that the two components are less correlated in the range of temperatures where their densities and viscosities are close. On the other hand, they are more correlated when the density of one of the components dominates. One can understand this as "slaving" of the rare component by the dense one that dominates the composition. When the two components are close in densities, each can have a life of its own, reducing the measured correlations between them.

A significant enhancement of small-scale intermittency, characterized by flatness, is observed in the intermediate temperature range $T = 1.8$–$2.0\,\mathrm{K}$. We suggest a flip-flop mechanism of such an enhancement. The efficient energy exchange between two components by mutual friction serves as an effective forcing on a wide range of scales. This forcing effectively intervenes with the energy cascade over scales. This effect is simultaneously present in both components. This observation confirms previous numerical results [16,18].

Given the present available resolution, it is difficult to make any systematic assessment about existence of pure inertial range scaling exponents which is independent of the Reyonlds number. Accordingly we cannot state whether these are different from the ones measured in homogeneous and isotropic classical turbulence. Usual phenomenology would predict that the mutual friction should induce some subleading scaling corrections that might indeed be the reasons for the apparently different scaling properties measured for some temperature range. Only further studies at increasing Reynolds numbers might be able to answer this question and clarify whether the differences between the two fluids and the apparently different scaling properties in the inertial range are Reynolds independent or not. On the other hand, the empirically observed enhancement of flatness at scales adjacent to the Kolmogorov microscale for the Reynolds numbers investigated here is a robust observation, independent of the existence of any power law scaling.

It is important to stress that in this paper we do not attempt to perform a systematic investigation of the robustness of the statistical and scaling properties as a function of the three dimensionless control parameters in the equations: the two Reynolds numbers and the ratio among the mutual

friction and the energy flux. Such a study is important and it will be reported elsewhere. Concerning the parameters explored within this study, the intermittency enhancement is a robust effect as verified by exploring smaller resolution DNS at 256^3 collocation points (not shown).

A possible reason for lack of experimental evidence of a temperature dependence of turbulent statistics in coflowing ^{4}He in Ref. [11] may be a particular choice of the flow type, which is anisotropic and in which the turbulence is not fully developed at small scales, where the effect is observed. Another possible reason is the finite size of the used probes, which prevented exploring smaller scales close to the mesoscopic quantum scale and the Kolmogorov viscous microscale, at which we observed such a dependence. Experiments that can target such scales might be able to verify our numerical results. The velocity flatness measurements in visualization experiments, such as Refs. [10,12,14], may provide an invaluable information about intermittency in superfluid turbulence at small scales.

ACKNOWLEDGMENTS

We acknowledge funding from the Prace project "Superfluid Turbulence under Counter-flows" (Pra12_ 3088). L.B. and G.S. acknowledge funding from the European Union's Seventh Framework Programme (No. FP7/2007-2013) under Grant Agreement No. 339032. We acknowledge useful discussions with L. Skrbek.

[1] C. F. Barenghi, L. Skrbek, and K. R. Sreenivasan, Introduction to quantum turbulence, Proc. Natl. Acad. Sci. USA **111**, 4647 (2014).
[2] H. E. Hall and W. F. Vinen, The rotation of liquid helium II, I: Experiments on the propagation of second sound in uniformly rotating helium II, Proc. R. Soc. London, Ser. A **238**, 204 (1956).
[3] I. L. Bekarevich and I. M. Khalatnikov, Phenomenological derivation of the equations of vortex motion in He II, Sov. Phys. JETP **13**, 643 (1961).
[4] J. Maurer and P. Tabeling, Local investigation of superfluid turbulence, Europhys. Lett. **43**, 29 (1998).
[5] J. Salort, C. Baudet, B. Castaing, B. Chabaud, F. Daviaud, T. Didelot, P. Diribarne, B. Dubrulle, Y. Gagne, F. Gauthier, A. Girard, B. Hébral, B. Rousset, P. Thibault, and P.-E. Roche, Turbulent velocity spectra in superfluid flows, Phys. Fluids **22**, 125102 (2010).
[6] J. Salort, B. Chabaud, E. Lévêque, and P.-E. Roche, Investigation of intermittency in superuid turbulence, J. Phys.: Conf. Ser. **318**, 042014 (2011).
[7] P.-E. Roche, C. F. Barenghi, and E. Lévéque, Quantum turbulence at finite temperature: The two-fluids cascade, Europhys. Lett. **87**, 54006 (2009).
[8] C. F. Barenghi, V. S. L'vov, and P.-E. Roche, Experimental, numerical, and analytical velocity spectra in turbulent quantum fluid, Proc. Natl. Acad. Sci. USA **111**, 4683 (2014).
[9] V. Eltsov, R. Hanninen, and M. Krusius, Quantum turbulence in superfluids with wall-clamped normal component, Proc. Natl. Acad. Sci. USA **111**, 4711 (2014).
[10] P. Švančara and M. La Mantia, Flows of liquid 4He due to oscillating grids, J. Fluid Mech. **832**, 578 (2017).
[11] E. Rusaouen, B. Chabaud, J. Salort, and P.-E. Roche, Intermittency of quantum turbulence with superfluid fractions from 0% to 96%, Phys. Fluids **29**, 105108 (2017).
[12] E. Varga, J. Gao, W. Guo, and L. Skrbek, Intermittency enhancement in quantum turbulence (unpublished).
[13] B. Dubrulle (private communication).
[14] M. La Mantia, P. Švančara, D. Duda, and L. Skrbek, Small-scale universality of particle dynamics in quantum turbulence, Phys. Rev. B **94**, 184512 (2016).
[15] M. La Mantia, Particle dynamics in wall-bounded thermal counterflow of superfluid helium, Phys. Fluids **29**, 065102 (2017).
[16] L. Boué, V. S. L'vov, A. Pomyalov, and I. Procaccia, Enhancement of Intermittency in Superfluid Turbulence, Phys. Rev. Lett. **110**, 014502 (2013).
[17] V. Shukla and R. Pandit, Multiscaling in superfluid turbulence: A shell-model study, Phys. Rev. E **94**, 043101 (2016).

[18] G. Krstulovic, Grid superfluid turbulence and intermittency at very low temperature, Phys. Rev. E **93**, 063104 (2016).
[19] R. J. Donnelly and C. F. Barenghi, The observed properties of liquid helium at the saturated vapor pressure, J. Phys. Chem. Ref. Data **27**, 1217 (1998).
[20] L. Biferale, D. Khomenko, V. L'vov, A. Pomyalov, I. Procaccia, and G. Sahoo, Local and non-local energy spectra of superfluid ^{3}He turbulence, Phys. Rev. B **95**, 184510 (2017).
[21] V. S. L'vov, S. V. Nazarenko and G. E. Volovik, Energy spectra of developed superfluid turbulence, JETP Lett. **80**, 535 (2004).
[22] S. R. Stalp, L. Skrbek, and R. J. Donnelly, Decay of Grid Turbulence in a Finite Channel, Phys. Rev. Lett. **82**, 4831 (1999).
[23] W. F. Vinen, Classical character of turbulence in a quantum liquid, Phys. Rev. B **61**, 1410 (2000).
[24] W. F. Vinen and J. J. Niemela, Quantum turbulence, J. Low Temp. Phys. **128**, 167 (2002).
[25] L. Boué and V. S. L'vov, Y. Nagar, S. V. Nazarenko, A. Pomyalov, and I. Procaccia, Energy and vorticity spectra in turbulent superfluid 4He from T = 0 to T_λ, Phys. Rev. B **91**, 144501 (2015).
[26] V. S. Lvov, S. V. Nazarenko, and O. Rudenko, Bottleneck crossover between classical and quantum superfluid turbulence, Phys. Rev. B **76**, 024520 (2007).
[27] V. S. Lvov, S. V. Nazarenko, and O. Rudenko, Gradual eddy-wave crossover in superfluid turbulence, J. Low Temp. Phys. **153**, 140 (2008).
[28] V. S. L'vov and A. Pomyalov, Statistics of quantum turbulence in superfluid He, J. Low Temp. Phys. **187**, 497 (2017).
[29] V. S. L'vov and I. Procaccia, Exact resummations in the theory of hydrodynamic turbulence, 1: The ball of locality and normal scaling, Phys. Rev. E **52**, 3840 (1995).
[30] V. S. L'vov and I. Procaccia, Exact resummations in the theory of hydrodynamic turbulence, 2: A ladder to anomalous scaling, Phys. Rev. E **52**, 3858 (1995).
[31] A. N. Kolmogorov, Dissipation of energy in the locally isotropic turbulence, Dokl. Akad. Nauk. SSSR **32**, 16 (1941).
[32] V. S. L'vov, E. Podivilov, and I. Procaccia, Exact result for the third order correlations of velocity in turbulence with helicity, arXiv:chao-dyn/9705016 v2.
[33] U. Frisch, *Turbulence: The Legacy of A. N. Kolmogorov* (Cambridge University Press, Cambridge, UK, 1995).
[34] V. S. Lvov, S. V. Nazarenko, and L. Skrbek, Energy spectra of developed turbulence in helium superuids, J. Low Temp. Phys. **145**, 125 (2006).
[35] R. Benzi, S. Ciliberto, R. Tripiccione, C. Baudet, F. Massaioli, and S. Succi, Extended self-similarity in turbulent flows, Phys. Rev. E **48**, R29(R) (1993).
[36] Z.-S. She and E. Leveque, Universal Scaling Laws in Fully Developed Turbulence, Phys. Rev. Lett. **72**, 336 (1994).